arXiv:nucl-ex/0109005v1 10 Sep 2001

Hard photon and neutral pion production in cold nuclear matter

L. Aphecetche [a,1], J. Bacelar [b], H. Delagrange [a,1], D. d'Enterria [a,1], M. Hoefman [b], H. Huisman [b], N. Kalantar-Nayestanaki [b], H. Löhner [b], G. Martínez [a,1], T. Matulewicz [c], J. Messchendorp [b], M.-J. Mora [a,1], R. Ostendorf [b], S. Schadmand [b,2], Y. Schutz [a,1], M. Seip [b], A. Taranenko [d], R. Turrisi [a,3], M.-J. Van Goethem [b,4], M. Volkerts [b], V. Wagner [d], H.W. Wilschut [b]

[a] *Grand Accélérateur National d'Ions Lourds, IN2P3-CNRS, DSM-CEA, BP 5027, 14076 Caen Cedex 5, France*

[b] *Kernfysisch Versneller Instituut, NL-9747 AA Groningen, The Netherlands*

[c] *Institute of Experimental Physics, Warsaw University, PL-00681 Warsaw, Poland*

[d] *Institute of Nuclear Physics, CZ-25068 Řež, Czech Republic*

Abstract

The production of hard photons and neutral pions in 190 MeV proton induced reactions on C, Ca, Ni, and W targets has been for the first time concurrently studied. Angular distributions and energy spectra up to the kinematical limit are discussed and the production cross-sections are presented. From the target mass dependence of the cross-sections the propagation of pions through nuclear matter is analyzed and the production mechanisms of hard photons and primordial pions are derived. It is found that the production of subthreshold particles proceeds mainly through first chance nucleon-nucleon collisions. For the most energetic particles the mass scaling evidences the effect of multiple collisions.

Key words: proton-nucleus reactions, hard photons, subthreshold pions
PACS: 21.65.+f, 25.75.Dw, 25.40.Qa

1 Introduction

Forming hot and compressed nuclear matter by colliding heavy ions provides the today only known experimental mean to explore the phase diagram of nuclear matter. During the collision the longitudinal momentum of the projectile is converted by multiple nucleon-nucleon collisions into transverse momentum as well as through the production of secondary particles, leading to the creation of a hot and compressed reaction zone. At projectile energies below the free pion production threshold ($E_{NN}^{th(\pi^o)}$=280 MeV) pions and hard photons ($E_\gamma \geq 30$ MeV) carry information on the initial compressional and high density phase of the heavy-ion collision which might evolve towards a hot thermalized nuclear system [1,2].

In first order, subthreshold pions and photons are created following either single or several nucleon-nucleon collisions, the nuclear medium providing the additional energy needed to surpass the production threshold. Therefore subthreshold pions and photons can be viewed as a snapshot of the dynamical phase-space occupancy of participant nucleons at the early instant of the collision. However, extracting the information relevant to the thermodynamical state of the system is far from being straightforward. One must rely on models which describe the complicated many-body problem of a heavy-ion collision. Alternatively, a purely empirical approach consists in the comparison of various observables between heavy-ion collisions and proton-nucleus collisions. Since a compressional phase is very unlikely to occur in the latter, the in-medium nucleon-nucleon collisions, i.e. the longitudinal momentum dissipation, can be studied without the complication due to the dynamics and thermodynamics of heavy-ion collisions.

For the present measurement the proton beam energy was chosen to be 190 MeV, resulting from a compromise between the concurrent requirements to accumulate a usable set of data and to be well below the pion production threshold. The energy spectra, up to the maximum energy available in the reaction for the production of a single particle, were measured together with their angular distributions. The target mass dependence of the production cross sections, studied as a function of the energy of the produced particle, is exploited to characterize the production mechanism and, in the case of pions, their propagation properties through nuclear matter. It is concluded that the production mechanism of subthreshold particles changes with increasing particle energy from a production in individual nucleon-nucleon collisions to

[1] Present address: SUBATECH, 4 rue A. Kastler, F-44307 Nantes, France
[2] Present address: II. Physikalisches Institut, Universität Gießen, D-35392 Gießen, Germany
[3] Present address: INFN-Padova, Via Marzolo 8, 35131 Padova, Italy
[4] Present address: NSCL, MSU, East Lansing, Michigan 48824-1321. USA.

mechanisms involving more than two nucleons. Although several similar studies have been published earlier [3-8], the information collected in the present work is unique as it combines for the first time the measurement of complete energy spectra with the concurrent observation of strongly interacting particles, pions, and non-interacting particles, photons.

2 Experimental setup

The 190 MeV proton beam was delivered by the superconducting cyclotron AGOR at KVI. Natural C, Ca, Ni and W targets, respectively 18.1, 11.2, 6.7 and 5.0 mg/cm^2 thick, were irradiated with 10 to 25 nA beams in bunches of 2 ns at a rate of 60 MHz. Within these conditions the interaction rate was respectively for the four targets 0.23, 0.13, 0.09, and 0.05 nuclear interactions per beam pulse. These values set the counting rate in an individual photon detection module to 1 kHz and induced negligible double hits and random coincidences. Direct photons and decay photons from neutral pions ($\pi^o \rightarrow \gamma\gamma$, BR=98.8%) were detected with the photon spectrometer TAPS configured in six blocks of 64 BaF_2 modules, each module being associated with a charged-particle-veto detector. The blocks were positioned at the most forward angles, allowed by technical constraints, on both sides of the beam. They covered a quasi-continuous polar angle range above $\theta = 60^o$ and an azimuthal angle range of $\pm 20^o$, hence covering approximately 15% of 4π. The distance from the target to the active front face of the blocks ($d = 66$ cm) offered a flight path large enough to discriminate photon hits against baryon (mainly neutron and proton) hits through their time-of-flight measurement. The energy deposited in the BaF_2 modules was calibrated and the gain continuously monitored during the experiment using the 38.5 MeV peak energy-deposition of cosmic muons. Time-of-flight was calibrated using the prompt photon signal and the known time interval between proton beam pulses (16.7 ns). To enrich the recorded events with photons and neutral pions the trigger electronics was set up to select events in which at least one, respectively two, neutral hits (defined as a hit in a BaF_2 module and no hit in the charged-particle-veto detector) were present, depositing at least 15 MeV equivalent photon energy. A downscaled trigger consisting of a neutral hit of at least 0.4 MeV served as minimum-bias trigger. An exhaustive description of the TAPS detector, its associated electronics and trigger scheme can be found in [2].

In the offline analysis photon hits were identified by combining the information delivered by the BaF_2 modules and by exploiting the characteristic pulse shape and time of flight of photons. The direction and energy of the impinging photon was derived from the analysis of the electromagnetic-shower topology[3,4] which provided also additional discrimination criteria against baryons and cosmic muons. Neutral pions were identified, with a full width at

half maximum of 10%, through an invariant mass analysis of identified photon pairs. In the resulting invariant mass spectrum combinatorial background can be safely neglected because of the weak γ multiplicity at the considered bombarding energies ($M_\gamma \approx 10^{-3}$). Photon pairs with an invariant mass between 100 and 160 MeV were adopted as stemming from the decay of the produced neutral pions. Close to one million pions were detected and identified for each target.

For every identified neutral pion, the 4-momentum was calculated through a constrained minimization method using the 4-momentum of the two photons. This special energy reconstruction method was developed[5] because the standard technique[6] leads to unphysical results[7] (pion energies above the kinematical limit) in our case, where the pions i) are of very low energy and ii) take away a large (up to 100%) part of the total energy available in the proton+nucleus system. Performances of this new method have been carefully checked using GEANT simulations[8] of mono-energetic neutral pions. Unlike the standard method, our minimization method leads to a non-symmetric response function (Fig. 1), with a reconstructed mean energy which is about 88% of the true value, and an energy resolution depending on pion energy (Fig. 1).

The neutral pion efficiency was calculated with the help of GEANT simulations taking as input an extrapolation $D(K_{\pi^o}, \Omega_{\pi^o})$ to the full solid angle of the measured double differential cross-sections $d^2\sigma/d\Omega_{\pi^o}dK_{\pi^o}$. $D(K_{\pi^o}, \Omega_{\pi^o})_{lab} = d\sigma/dK_{\pi^o}$ (angular distribution has been chosen isotropic, in agreement with the data) where $d\sigma/dK_{\pi^o}$ was obtained through the following iterative procedure. The distribution of the measured kinetic energy, K_{π^o}, was parametrized as :

$$\frac{d\sigma}{dK_\pi} \propto K_{\pi^o}^{\alpha} \times \exp\left(-\frac{K_{\pi^o}}{T_1}\right) \times \frac{1}{1+\exp\left(\frac{K_{\pi^o}-K_0}{T_2}\right)} \qquad (1)$$

Expression 1 was selected as the initial guess of the iteration procedure and fed into the simulation. The parameters α, T_1, T_2, K_0 were then tuned until the output of the simulation reproduces the measured distribution.

The photon efficiency was calculated using the same scheme, with the following input distribution :

$$\left(\frac{d^2\sigma_\gamma}{dE_\gamma\Omega_\gamma}\right)_{NNcm}^{E_\gamma>40MeV} \propto \exp\left(\frac{E_\gamma - E_0}{\sigma_E}\right) \times \left[\alpha_1 \sin^2(\theta_\gamma) + \alpha_2\right]$$

The resulting pion and photon efficiencies are reported in Table 1.

3 Cross-sections

The neutral pion total cross sections were calculated as:

$$\sigma_{\pi^o}^{4\pi} = \mathcal{C}_D \times N_{\pi^o}^{raw} / \epsilon_{\pi^o}^{4\pi}$$

where $N_{\pi^o}^{raw}$ is the raw number of identified pions, $\mathcal{C}_D$ is a normalization factor including target thickness, beam intensities and trigger conditions, and $\epsilon_{\pi^o}^{4\pi}$ is the global efficiency. The resulting cross-sections $\sigma_{\pi^o}^{4\pi}$ are reported in Table 1.

To obtain direct photon cross-sections an additional treatment is required, as the contribution of the decay photons from neutral pions must be subtracted from the total photon cross-section. The latter is obtained as

$$\sigma_\gamma = \mathcal{C}'_D \times N_\gamma^{raw} / \epsilon_\gamma^{4\pi}$$

where $\epsilon_\gamma^{4\pi} = 12\%$ is the efficiency for photons and N_γ^{raw} is the raw number of identified photons. The contribution of the decay photons was estimated with the help of GEANT simulations taking as input the extrapolated double-differential cross-section $D(K_{\pi^o}, \Omega_{\pi^o})$. The contribution of decay photons amounts to about 30% of the photon spectrum (Fig. 3).

From the photon cross section the probability P_γ to produce a single photon in an individual proton-neutron collision was evaluated according to the prescription of [9]. We observe a good agreement of this probability with the systematics presented in [9] (averaged for Ca, Ni, W targets, the P_γ equals to $(7.4 \pm 1.4) \times 10^{-4}$, compared to 9.4×10^{-4} expected from the systematics) with the exception of the C target (factor 2 below the systematics). The neutral pion cross sections can be compared to the results of [10] obtained with proton beams of 200 MeV kinetic energy. While we observe the same (within error bars) mass scaling law of the total cross section for neutral pion production, the cross section values reported in [10] are higher by a factor of approximately 3. Such a strong rise can not be attributed to the 10 MeV difference in beam energies. The problem of inconsistencies in the cross section for pion production in proton-nucleus reactions is discussed in detail in [11].

Thanks to the good statistics accumulated, errors in this experiment are mainly systematic in nature, and amount to 10% for $\mathcal{C}_D$, 7% for $\epsilon_{\pi^o}^{4\pi}$, 20% for $\epsilon_\gamma^{4\pi}$, leading to total relative errors of about 32% for the direct photon cross sections and 12% for the total pion cross sections.

The energy spectra of particles (Figs. 2 and 3) produced from the four different targets are conveniently compared if one defines a reduced energy, e_r, which represents the fraction of the available kinetic-energy, K^{max}, carried away by

the particle. This energy is calculated (Table 2) assuming that the reaction proceeds through the fusion of the proton and the target nucleus: $K^{max} = \sqrt{s} - (A+1)\,M_N - Q$, where $\sqrt{s}$ represents the total energy available in the center-of-mass, M_N the nucleon mass and Q the fusion reaction Q-value. For photons $K \equiv E_\gamma$. Within this representation (Figs. 2 and 3, right panels) particles with $e_r = 1$ take away all the available energy and the mechanism would be pionic fusion[12] for pions or radiative capture for photons.

4 Analysis of target mass dependence

The dependence with the target mass A of the pion and photon cross-sections can be described by a power law, $d\sigma/dx \propto A^{\alpha(x)}$, where x is either the polar angle of the emitted particle or its reduced kinetic energy. This widely used parametrization at relativistic [13–16] as well as ultrarelativistic [17,18] energies for a variety of produced particles gives valuable indications on the particle-production mechanism. Since one is interested in the primordial particle production, one must first understand how the primordial production is modified by subsequent absorption or re-scattering during the propagation through the nuclear medium. This has been done by examining the target mass dependence of the differential cross-section, $d\sigma/d\theta_{\pi^o}$, in terms of an elementary geometrical model which tracks the pion through the nucleus after its creation [5]. Within this picture our data are best described if one assumes that: i) primordial pions are produced in a surface shell of the nucleus with thickness $\lambda_p = 2.4$ fm, which is equal to the proton mean free path, and ii) the pion mean free path, independent of the pion energy, is equal to $\lambda_\pi = 6$ fm in good agreement with the values established elsewhere [19]. The first assumption implies that pions detected in the backward hemisphere are quasi unaffected by re-interaction in the medium and those pions can thus be considered as primordial pions.

The target mass A dependence of neutral pion and photon cross-sections was analyzed in terms of the power-law parameter α. The carbon data have been excluded from this analysis because of its extraordinary behavior (see also [20]). All neutral pions and photons with energy above 92 MeV were produced below the free NN threshold. For hard photons produced below threshold the α parameter (Fig. 4) continously increases from $\alpha = 2/3$ to values close to or even above one. This behavior is interpreted as an evolution of the particle-production mechanism from a surface production for the least energetic particles towards a volume production for the most energetic particles. In other words, the observed α dependence witnesses a transition from particles produced in first-chance nucleon-nucleon collisions to particles produced in multiple successive binary collisions. A possible mechanism for the latter is the process of photoabsorption of subthreshold pions in the nuclear

medium ($NN \rightarrow NN\pi$ and subsequently $N\pi \rightarrow N\gamma$), as proposed in [21]. The α dependence with the photon energy (Fig.4) indicates another strong rise when the energy of photons decreases. This can be understood invoking again the participation of all nucleons with the difference that in this case there is enough energy available, not only in first chance collisions but also in secondary collisions. A detailed analysis of this photon energy region was performed by another TAPS experiment during the same experimental campaign at KVI [20].

In the case of neutral pions such firm conclusions can not be drawn from the available experimental data. Within error bars, a rise of the α parameter towards unity or a constant value of $\alpha = 2/3$ can not be distinguished. It must be emphasized that, compared to photons, pions are less adequate probes for a model-independent analysis. Their production often involves baryonic resonances as intermediate steps [22], and the energy dependence of the power-law parameter α might be affected by the energy variation of the pion absorption length, an effect not accounted for in the simple geometrical model used here.

5 Conclusion

A complete data set on the production of neutral pions and photons in reactions of 190 MeV protons with targets ranging in mass from $A = 12$ to $A = 184$ has been obtained. Energy spectra up to the kinematical limit have been presented. A simple geometrical model, assuming neutral pion production in a surface shell of the target nucleus and subsequent pion propagation with the mean free path equal to $\lambda_\pi = 6$ fm, agrees well with the observed angular distribution of neutral pions. The analysis of the mass scaling law of subthreshold particle cross-sections supports the mechanism of particle production in first-chance nucleon-nucleon collisions, except in the case of most energetic particles (up to the kinematical limit), where the role of multi-step processes becomes evident.

The present data furnish new and valuable information for tuning unknown parameters of dynamical models for heavy-ion collisions[1], like in-medium cross sections or the implementation of the Pauli principle. Further evidence for new production mechanisms like $pn \rightarrow d\pi\,(\gamma)$ or $\pi N \rightarrow N\gamma$ [21] has been given. The complicated and hardly understood production mechanism of hadronic particles, like pions and kaons [23], affected by reabsorption and rescattering, stresses the importance of hard-photon measurements as presented in this letter. Once hadronic and electromagnetic probes are well understood, the dynamical transport model codes may provide a better description of the particle production in heavy-ion collisions, which is the base to unravel the thermodynamic properties of nuclear matter.

Acknowledgements

We would like to thank the AGOR team for providing a high quality proton beam. This work was in part supported by the Institut National de Physique Nucléaire et de Physique des Particules, France, by the Dutch Stichting voor Fundamenteel Onderzoek der Materie, The Netherlands, and by the Grant Agency of the Czech Republic.

References

[1] W. Cassing, V. Metag, U. Mosel, and K. Niita, Phys. Rep. **188**, 363 (1990).

[2] Y. Schutz *et al.*, Nucl. Phys. **A622**, 405 (1997).

[3] G. Martínez *et al.*, Nucl. Inst. and Meth. **A391**, 435 (1997).

[4] F. Marqués *et al.*, Nucl. Inst. and Meth. A **365**, 392 (1995).

[5] L. Aphecetche, Ph.D. thesis, Université de Caen, GANIL Report T98-03, 1998.

[6] H. Baer *et al.*, Nucl. Inst. and Meth. **180**, 445 (1981).

[7] K. Korzecka and T. Matulewicz, Nucl. Inst. and Meth. **A453**, 606 (2000).

[8] L. Aphecetche *et al.*, GANIL Report **R9702**, 1 (1997).

[9] J. Clayton *et al.*, Phys. Rev. **C45**, 1815 (1992).

[10] V. Bellini *et al.*, Z. Phys. **A333**, 393 (1989).

[11] H. Wilschut, M.-J. van Goethem, H. Löhner, and R. Ostendorf, submitted to Phys. Rev. C.

[12] D. Horn *et al.*, Phys. Rev. Lett. **77**, 2408 (1996).

[13] R. Elmér *et al.*, Phys. Rev. Lett. **77**, 4884 (1996).

[14] A. Wolf *et al.*, Phys. Rev. Lett. **80**, 5281 (1998).

[15] D. Miskowiec *et al.*, Phys. Rev. Lett. **72**, 3650 (1994).

[16] R. Bath *et al.*, Phys. Rev. Lett. **78**, 4007 (1997).

[17] R. Albrecht *et al.*, Eur. Phys. J. **C5**, 255 (1998).

[18] M. Aggarwal *et al.*, Phys.Rev.Lett. **81**, 4087 (1998).

[19] R. Mayer *et al.*, Phys. Rev. Lett. **70**, 904 (1993).

[20] M.-J. V. Goethem, Ph.D. thesis, Rijkuniversiteit Groningen, The Netherlands, 2000.

[21] K. K. Gudima *et al.*, Phys. Rev. Lett. **76**, 2412 (1996).

[22] T. Matulewicz *et al.*, Eur. Phys. J **A9**, 69 (2000).

[23] V. Koptev *et al.*, Phys. Rev. Lett. **87**, 022301 (2001).

[24] G. Audi, O. Bersillon, J. Blachot, and A. Wapstra, Nucl. Phys. **A624**, 1 (1997).

Table 1
Cross sections of neutral pions and photons measured in p+A reactions at 190 MeV. $N_{\pi^o}^{raw}$ is the number of neutral pions recorded, $\mathcal{C}_D$ takes into account target thickness, beam intensity and trigger rates. $\sigma_{\pi^o}^{4\pi} = \mathcal{C}_D \times N_{\pi^o}^{raw}/\epsilon_{\pi^o}^{4\pi}$ is the total neutral pion cross-section, calculated using estimated neutral pion global efficiency. The direct photon cross-section $\sigma_\gamma^{direct} = \sigma_\gamma^{total} - \sigma_\gamma^{\pi^o \to \gamma\gamma}$ is then deduced from the total photon cross-section by subtracting contribution from decay photons. All photon cross-sections are given for $E_\gamma^{lab} \geq 40$ MeV.

	C	Ca	Ni	W
$\mathcal{C}_D \times 10^6$ (μb)	1.45 ± 0.15	10.2 ± 1.0	2.38 ± 0.24	12.5 ± 1.2
$N_{\pi^o}^{raw} \times 10^{-5}$	3.042 ± 0.005	2.017 ± 0.004	9.870 ± 0.01	4.166 ± 0.006
$\epsilon_{\pi^o}^{4\pi}$ (%)	2.65 ± 0.18	2.43 ± 0.18	2.43 ± 0.18	2.44 ± 0.18
$\sigma_{\pi^o}^{4\pi}$ (μb)	16 ± 2	85 ± 10	97 ± 12	215 ± 26
$\epsilon_\gamma^{4\pi}$ (%)	0.12 ± 0.02	0.12 ± 0.02	0.12 ± 0.02	0.12 ± 0.02
σ_γ^{total} (μb)	88 ± 20	520 ± 120	567 ± 130	1383 ± 320
$\sigma_\gamma^{\pi^o \to \gamma\gamma}$ (μb)	28 ± 3	149 ± 18	170 ± 20	376 ± 45
σ_γ^{direct} (μb)	60 ± 20	372 ± 120	397 ± 130	1007 ± 310

Table 2
Reaction Q-values (from [24]), used to compute the maximum available K_{max} in A(p,X) reactions : $Q_{gg} = \Delta M_{A+1} - \Delta M_A - \Delta M_1 + m_X$ where $X = \pi^o, \gamma$.

Reaction	Q_{gg} (MeV)	K_{max} (MeV)
${}^{12}_{6}\mathrm{C}_{g.s.}(p,\pi^0){}^{13}_{7}\mathrm{N}_{g.s.}$	133.0	41
${}^{40}_{20}\mathrm{Ca}_{g.s.}(p,\pi^0){}^{41}_{21}\mathrm{Sc}_{g.s.}$	133.9	51
${}^{58}_{28}\mathrm{Ni}_{g.s.}(p,\pi^0){}^{59}_{29}\mathrm{Cu}_{g.s.}$	131.5	55
${}^{184}_{74}\mathrm{W}_{g.s.}(p,\pi^0){}^{185}_{75}\mathrm{Re}_{g.s.}$	129.6	59
${}^{12}_{6}\mathrm{C}_{g.s}(p,\gamma){}^{13}_{7}\mathrm{N}_{g.s.}$	-1.94	176
${}^{40}_{20}\mathrm{Ca}_{g.s.}(p,\gamma){}^{41}_{21}\mathrm{Se}_{g.s.}$	-1.08	186
${}^{58}_{28}\mathrm{Ni}_{g.s.}(p,\gamma){}^{59}_{29}\mathrm{Cu}_{g.s.}$	-3.42	190
${}^{184}_{74}\mathrm{W}_{g.s.}(p,\gamma){}^{185}_{75}\mathrm{Re}_{g.s.}$	-5.40	194

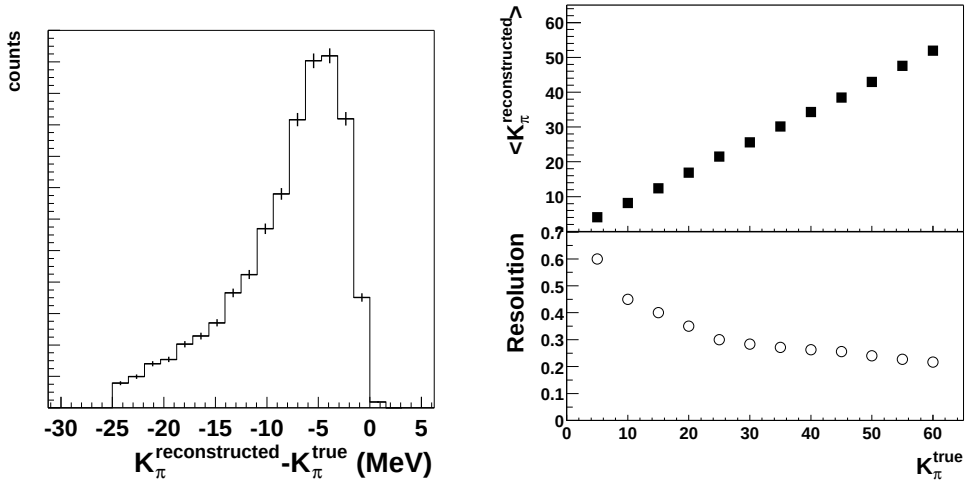

Fig. 1. Left: typical simulated response function of TAPS to mono-energetic neutral pions of 25 MeV, represented by the difference between the true initial pion kinetic energy and the reconstructed pion kinetic energy modified by the detection system and the reconstruction altogether. Right: Performance of the neutral pion momentum reconstruction method, as a function of the neutral pion kinetic energy (top: mean of the reconstructed energy, bottom: resolution).

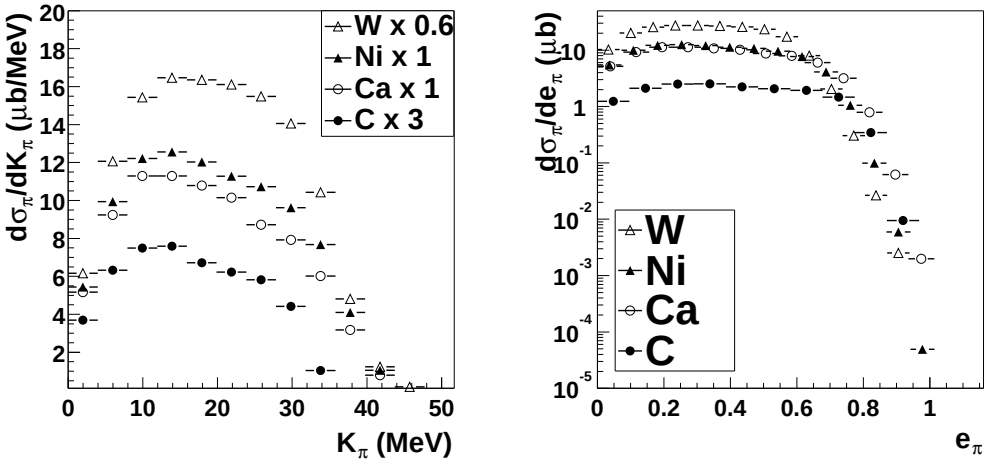

Fig. 2. Neutral pion energy spectra measured in p+A reactions at 190 MeV, as a function of kinetic pion energy (left) and of the reduced neutral pion energy $e_\pi = K_\pi/K^{max}$ (right, see text).

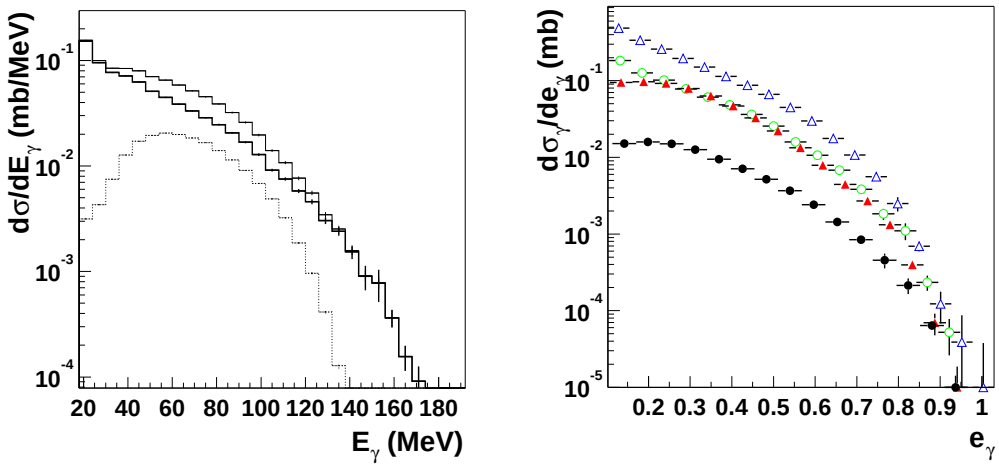

Fig. 3. Left: contribution of decay photons from π^0 (dotted line) in the total (thin solid line) photon spectra, and the resulting direct photon spectra (bold solid line). Right: direct photon energy spectra measured in p+A reactions at 190 MeV, as a function of the reduced photon energy (from bottom to top: C, Ca, Ni and W).

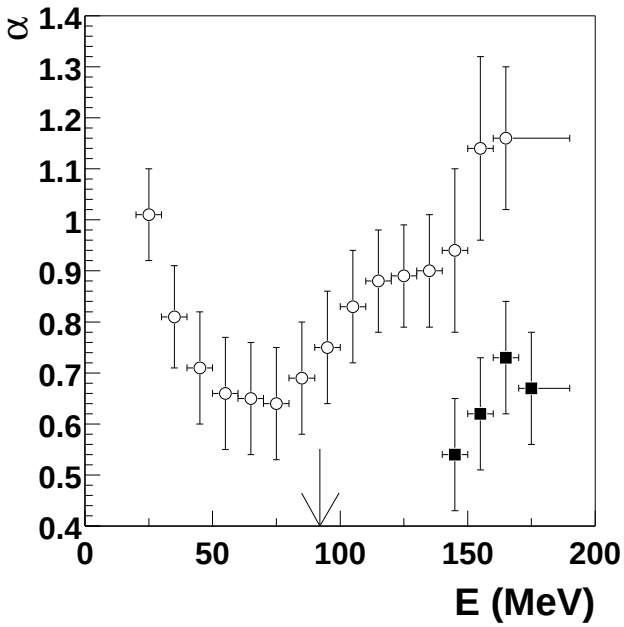

Fig. 4. Evolution of the α parameter as a function of the particle energy, for photons (open symbols) and neutral pions (closed symbols). The arrow indicates the separation between below- and above-threshold photons.